Article

Materials synthesis at terapascal static pressures

Leonid Dubrovinsky[1✉], Saiana Khandarkhaeva[1,2], Timofey Fedotenko[3], Dominique Laniel[2], Maxim Bykov[4], Carlotta Giacobbe[5], Eleanor Lawrence Bright[5], Pavel Sedmak[5], Stella Chariton[6], Vitali Prakapenka[6], Alena V. Ponomareva[7], Ekaterina A. Smirnova[7], Maxim P. Belov[7], Ferenc Tasnádi[8], Nina Shulumba[8], Florian Trybel[8], Igor A. Abrikosov[8✉] & Natalia Dubrovinskaia[2,8]

Theoretical modelling predicts very unusual structures and properties of materials at extreme pressure and temperature conditions[1,2]. Hitherto, their synthesis and investigation above 200 gigapascals have been hindered both by the technical complexity of ultrahigh-pressure experiments and by the absence of relevant in situ methods of materials analysis. Here we report on a methodology developed to enable experiments at static compression in the terapascal regime with laser heating. We apply this method to realize pressures of about 600 and 900 gigapascals in a laser-heated double-stage diamond anvil cell[3], producing a rhenium–nitrogen alloy and achieving the synthesis of rhenium nitride Re_7N_3—which, as our theoretical analysis shows, is only stable under extreme compression. Full chemical and structural characterization of the materials, realized using synchrotron single-crystal X-ray diffraction on microcrystals in situ, demonstrates the capabilities of the methodology to extend high-pressure crystallography to the terapascal regime.

The state of matter is strongly affected by variations in chemical composition and external parameters such as pressure and temperature, enabling tuning of material properties. This gives rise to various phenomena relevant for a broad range of scientific disciplines and technological applications, from fundamental understanding of the Universe to targeted design of advanced materials. Compression is known to facilitate metal-to-insulator transitions[4], superconductivity[5] and new 'super' states of matter[6]. Recent developments in the diamond anvil cell technique, and, particularly, the invention of double-stage and toroidal diamond anvil cells (dsDACs and tDACs)[3,7,8], have enabled breakthroughs in the synthesis of materials and the study of structure–property relationships at high and ultrahigh pressures. Very recent examples are the discovery of a new nitrogen allotrope[9], bp-N, which resolved a puzzle in our understanding of the high-pressure behaviour of pnictogen family elements, and the synthesis of a plethora of novel transition metal nitrides and polynitrides[10–15], including metal–inorganic frameworks[11,15], which are a new class of compounds featuring open porous structures at megabar compression. Solving and refining the crystal structures of solids synthesized directly from elements in laser-heated conventional DACs[10–15] at pressures as high as up to about two megabars[12,16] became possible owing to the synergy of our expertise both in generating pressures of several megabars[3,17,18] (for details see Supplementary Information section 'Brief overview of the double-stage DAC (dsDAC) technique') and in single-crystal X-ray diffraction (XRD) at ultrahigh pressures, which were pioneered a few years ago[19,20]. As the high-pressure high-temperature synthesis has become
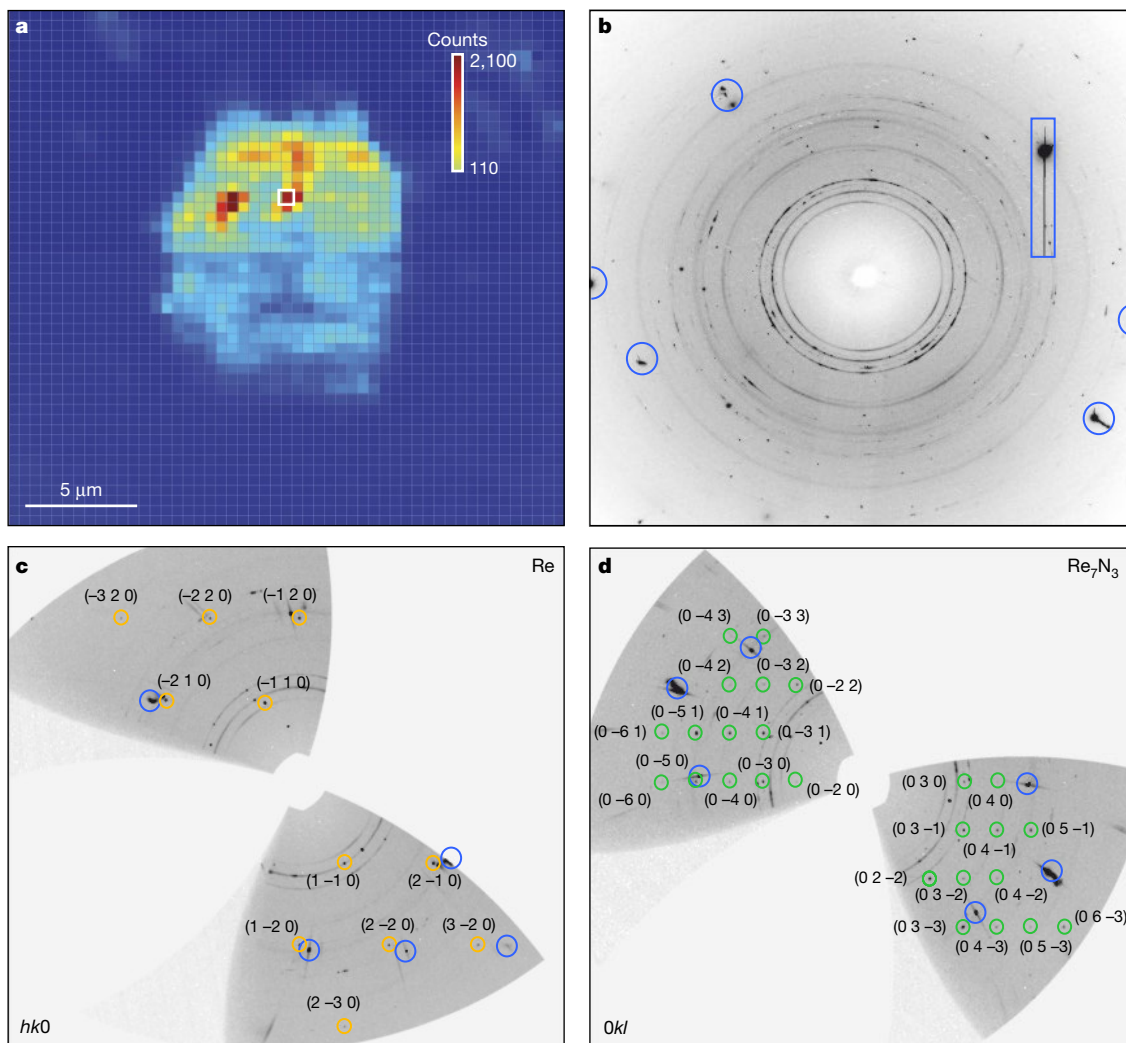
a well established technique for materials discovery, extending investigations to the TPa regime has long been desired.

Here we report a methodology for high-pressure high-temperature synthesis experiments that extends the limits of high-pressure crystallography to the terapascal range. To achieve the desired pressures, we combined toroidal[7,8] and double-stage[3,17,18] anvil designs. A rhenium–nitrogen alloy and rhenium nitride Re_7N_3 were synthesized in three different experiments in the Re–N system (Supplementary Table 1) in a laser-heated dsDAC. Their full structural and chemical characterization was performed in situ using single-crystal XRD.

The dsDACs were prepared following the procedure outlined below. Conventional Boehler–Almax-type single-bevelled diamond anvils with 40-µm culets were milled by focused ion beam (FIB) in order to produce a toroidal profile on the surface of the culet and to shape a miniature culet of about 10 µm in diameter in its centre (Extended Data Fig. 1). As a gasket we used a strip of a 200-µm-thick Re foil, which was pre-indented in a few steps. The final indentation of 10 µm in diameter (made using anvils with the toroidal profile) had a thickness of about 4 µm (the indentation procedure is described in detail in the legend to Extended Data Fig. 1). A hole of approximately 6 µm in diameter was made in the centre of the indentation using FIB or by tightly focused pulsed near-infrared laser to form a pressure chamber. A schematic of the dsDAC assembly, mounted into a BX-90 DAC[21] equipped with toroidal diamond anvils, is shown in Extended Data Fig. 1. To realize a dsDAC design, two transparent nanocrystalline diamond[17] hemispheres, FIB-milled from a single ball with a diameter of 12 to 14 µm,

Fig. 1 | Results of XRD measurements on the sample of Re and N_2 pulsed laser-heated in dsDAC #1. **a**, X-ray 2D map showing the distribution of different phases (recrystallized Re and Re_7N_3) in the pressure chamber of dsDAC #1. Each pixel on the map corresponds to a 2D XRD pattern collected at the Frelon 4M detector at the ID11 beamline at ESRF (beam size FWHM approximately 0.45×0.45 μm^2, $\lambda = 0.3099$ Å). The map covers the whole pressure chamber (21.5×21.5 μm^2, steps of 0.5 μm in both directions, 10-s acquisition time per frame). The total collection time was about 8 h. The colour intensity is proportional to the intensity of the following reflections: the (100) reflection of the Re gasket for the dark blue region; the (101) reflection of Re for the light blue region (inside the sample chamber); the inset colour bar

corresponds to the sum of intensities of (202) and (420) reflections of Re_7N_3. **b**, Example of an as-collected diffraction image with diffraction lines and spots of Re ($a = 2.2269(4)$ Å, $c = 3.5702(15)$ Å) and Re_7N_3 ($a = 6.2788(2)$ Å, $c = 4.000(2)$ Å). The characteristic diffraction image shown in **b** is highlighted with a white rectangle in **a**. **c**, **d**, The reconstructed reciprocal lattice planes of Re (**c**) and Re_7N_3 (**d**). In **c**, **d**, the reflections of Re and Re_7N_3 are marked by yellow and green circles, respectively, and the corresponding hkl are given. Powder diffraction lines are due to the Re gasket and untransformed rhenium. In **b**–**d**, blue circles and the blue rectangle indicate parasitic reflections from diamond anvils.

were placed over the tip of the 10-μm culet (Extended Data Figs. 1, 2). The hemispheres were small enough to stick on the toroidal anvils, but in one case (dsDAC #2, Supplementary Table 1) paraffin wax was used to affix them. A few grains of a rhenium powder (99.995% purity, Merck) were placed into the pressure chamber, which was then filled with nitrogen (N_2) at about 1.4 kbar using the high-pressure gas-loading set-up[22] at Bayerisches Geoinstitut (BGI, Bayreuth, Germany), closed, and pressurized.

After closing the cells in the pressure chambers, pressures were about 50 to 80 GPa (Extended Data Fig. 3); pressures on the primary anvils were below 10 GPa, as measured according to refs. [23,24]. Our experience suggests that the cell should be pressurized quickly to approximately 40 GPa on the primary anvils to avoid loss of nitrogen. The presence of nitrogen can be monitored on N_2 vibrons in the Raman spectra (Extended Data Fig. 3). However, N_2 vibrons were not detectable above approximately 150 GPa (Extended Data Fig. 3) in the pressure chamber,

because at such compression nitrogen becomes non-transparent and we can no longer detect the Raman signal. In dsDAC #2 we were able to observe the evolution of the Raman signal from the secondary anvil in parallel with that from the primary anvil upon pressurization (Extended Data Fig. 4). Huge stress on the secondary anvil is manifested in the large asymmetry of its corresponding Raman line, the high-frequency edge of which is difficult to determine reliably (Extended Data Fig. 4). Thus, it cannot be used for characterization of pressure in the sample chamber. (We also note that, as a rule, Raman spectra of nanocrystalline diamond are somewhat weak and broad).

In all dsDAC experiments described here, we followed the same protocol. After pressurization of the cells to about 120–140 GPa on the first-stage anvils[24], the samples were laser-heated. The dsDACs #2 and #3 were heated by a pulsed laser (1-μs pulse duration, 25-kHz repetition rate, approximately 25 W at each side) at BGI using the set-up specially designed for ultrahigh pressures: the near-infrared (1,070 nm) laser beam is of less than
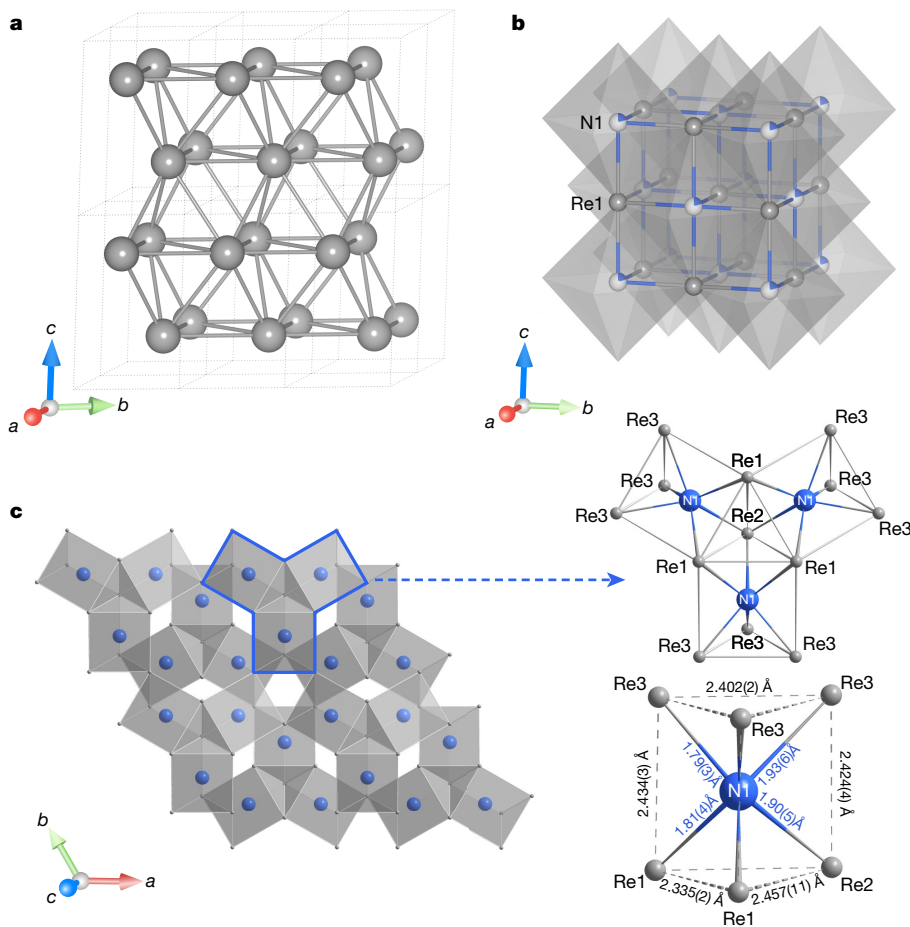
Fig. 2 | Crystal structures of the phases observed in laser-heated dsDACs. a, Hexagonal rhenium at 905(5) GPa in dsDAC #1 ($a = 2.2269(4)$ Å, $c = 3.5702(15)$ Å and $V = 15.33(1)$ Å^3). **b**, Cubic (B1 NaCl-type) rhenium–nitrogen solid solution ReN$_{0.2}$ at 730(4) GPa ($a = 3.3994(7)$ Å, $V = 39.28(2)$ Å^3). **c**, Hexagonal Re$_7$N$_3$ ($a = 6.2788(2)$ Å, $c = 4.000(2)$ Å and $V = 136.53(11)$ Å^3). In Re$_7$N$_3$, the structural units are NRe$_6$ prisms with the nitrogen atom in the centre. Rhenium atoms are grey and nitrogen atoms are blue.

5 μm full-width at half-maximum (FWHM) in diameter and has an optical magnification of about 300×[25,26]. The entire pressure chamber of dsDAC #2 was heated at 2,900(200) K for about 3 min, and dsDAC #3 at 3,450(200) K for about 5 min. After laser-heating, the pressures on the primary anvils of dsDAC #2 and dsDAC #3 were about 100 GPa and 120 GPa, respectively.

The dsDAC #1 was heated at 13-IDD at GSECARS (Advanced Photon Source, USA) from both sides using a tightly focused near-infrared laser beam (FWHM of about 8 μm in diameter) in pulsed mode (1-μs pulse duration, 50-kHz repetition rate, approximately 20 W each side) for 5 s at a temperature of 2,200(200) K. Powder diffraction data acquired before laser-heating (Extended Data Fig. 5; at 13-IDD the X-ray beam had a FWHM of approximately 3×3 μm^2) gave the following lattice parameters for Re: for the gasket, $a = 2.5606(5)$ Å, $c = 4.0588(12)$ Å, $V = 23.047(7)$ Å^3, and for the Re sample, $a = 2.2214(3)$ Å, $c = 3.5609(8)$ Å, $V = 15.21(1)$ Å^3. These parameters correspond to pressures of 149(3) GPa on the gasket and 930(5) GPa on the sample; the conservative values are given according to the equation of state from ref. [27] (Supplementary Table 1; the uncertainty in pressure corresponds to the statistical error in volume). X-ray powder diffraction patterns collected after laser-heating show the positions of the diffraction lines of the Re gasket did not change within the accuracy of the measurements, and those from the Re sample changed very slightly ($a = 2.2297(2)$ Å, $c = 3.5735(5)$ Å, $V = 15.38(1)$ Å^3) corresponding to a pressure of 895(5) GPa (ref. [27]).

After laser-heating for each dsDAC at 13-IDD at GSECARS, numerous diffraction spots were observed (Extended Data Fig. 5), indicating phase transformation(s) and/or chemical reaction(s) in the samples. However, interpreting the powder diffraction data turned out to be impossible, as the patterns were dominated by the diffraction lines from the gasket and untransformed Re, owing to the relatively large X-ray beam and a small sample size. Single-crystal diffraction data were of poor quality that precluded their analysis.

The dsDACs with temperature-quenched material were transported to ID11 at the European Synchrotron Radiation Facility (ESRF, Grenoble, France) and investigated using both powder and single-crystal XRD (see Methods). Despite the nominally small size of the X-ray beam, the reflections from the gasket were present even in the patterns collected from the centre of the sample chamber. Two-dimensional (2D) diffraction maps of still XRD images revealed powder diffraction of the Re gasket and untransformed material that enabled the analysis of the pressure distribution both within and around the sample (Extended Data Fig. 2). In dsDAC #1, for example, pressure at the sample/gasket boundary did not exceed approximately 160 GPa, and pressure at all points within the sample chamber was almost the same, of about 900 GPa (Extended Data Fig. 2). Our observations regarding the pressure distribution (Extended Data Fig. 3) in the sample chamber are consistent with those previously reported for toroidal-type anvils[7,8] and give the pressure magnification factor (the ratio of the pressures on the primary and secondary anvils) of about 6, in accordance with previous publications on ds-DACs[17,28].

Apart from powder diffraction rings, the diffraction patterns collected at ID11 from certain locations in the sample area show numerous spots (Fig. 1). At these positions we collected single-crystal datasets upon rotation of the DAC around the ω axis from −38° to 38° with an angular step of 0.5° (Methods). For dsDAC #1, particularly, the analysis of single-crystal XRD data revealed the presence of domains of two phases (Supplementary Table 2). The first phase is hexagonal (space group $P6_3/mmc$) with lattice parameters $a = 2.2269(4)$ Å, $c = 3.5702(15)$ Å and $V = 15.33(1)$ Å^3, as determined using 64 reflections. This was interpreted as Re (Figs. 1, 2) being under a pressure of 905(5) GPa (ref. [27]). Within uncertainty, the c/a ratio (1.603(5)) coincides with that reported for pure Re at lower pressures[3,27]. The structure solution and refinement showed indeed that rhenium recrystallizes upon pulsed laser-heating (Fig. 2 and
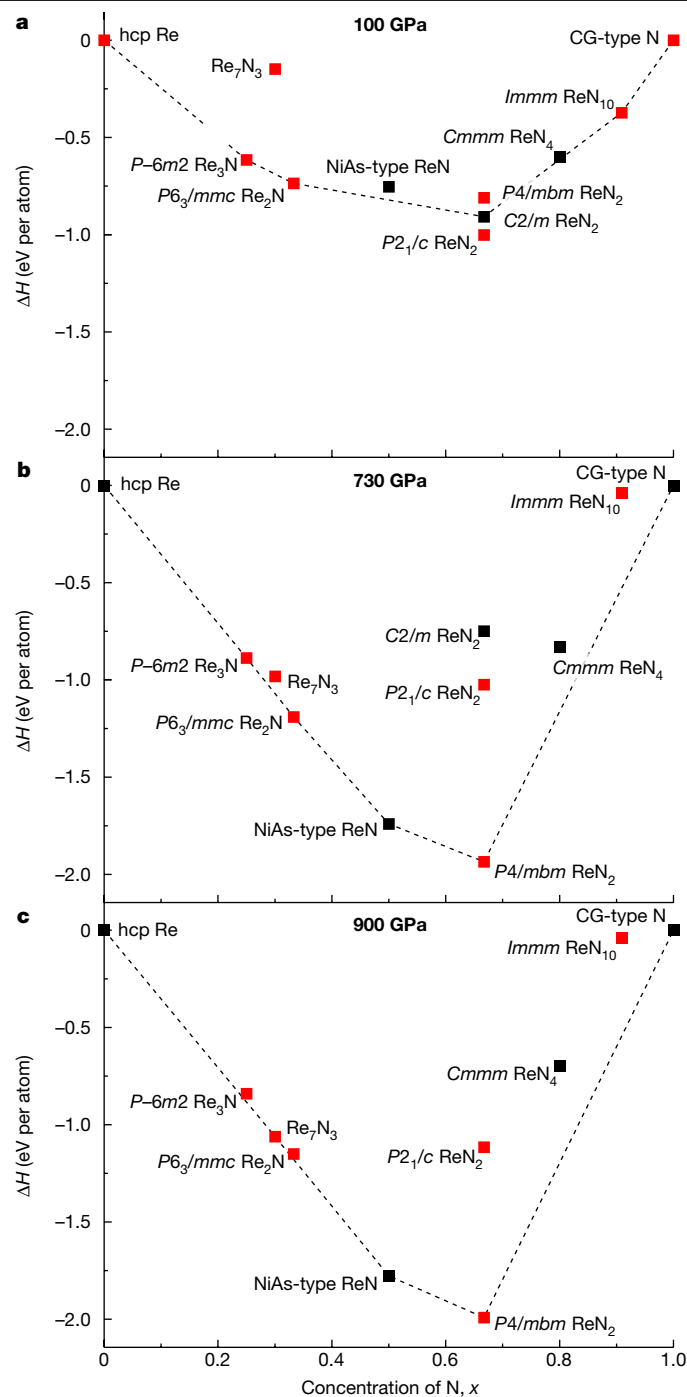
Fig. 3 | Formation enthalpy of Re₇N₃. a–c, Data are shown with respect to theoretically predicted[34] (black squares) and experimentally known (red squares, Re₃N and ReN₂[13] (P2₁/c), ReN₂ (P4/mbm), ReN₁₀[11] (Immm)) competing high-pressure phases in the ReN$_x$ system, calculated at pressures of 100 GPa (**a**), 730 GPa (**b**) and 900 GPa (**c**). hcp, hexagonal close-packed; CG-type N, cubic gauche nitrogen.

Supplementary Table 2), but is not contaminated by carbon or nitrogen (at least in the quantities that could be detectable from our XRD data).

The second phase found in the pressure chamber of the dsDAC #1 after heating is also hexagonal (space group P6₃mc) and has lattice parameters $a = 6.2788(2)$ Å, $c = 4.000(2)$ Å and $V = 136.53(11)$ Å³. On the basis of 394 independent reflections, the structure of this phase was solved and refined in isotropic approximation of atomic displacement parameters (Fig. 2 and Supplementary Table 2) to $R_1 = 5.7\%$. The chemical composition of the phase was refined as Re₇N₃. Considering the possibility of the

reaction between rhenium and carbon from the anvils, we checked if the phase could be interpreted as carbide (Re₇C₃). In this case, however, the isotropic thermal parameter of carbon becomes negative, supporting the assignment of the atomic positions to nitrogen.

The structure units of Re₇N₃ are distorted NRe₆ trigonal prisms (Fig. 2). Three prisms are connected through shared edges forming triads, which are stacked along the 6₃ axis. Each triad is rotated by 60° with regard to upper and lower neighbours in the columns (Fig. 2). The columns are connected to each other by the common vertices of the prisms. Crystal structures built of combined triads of prisms are well known among carbides, borides, phosphides and nitrides[29]. Moreover, there are a number of binary compounds with the A_7X_3 stoichiometry (A and X are different chemical elements), and especially hexagonal ones with Th₇Fe₃-type structure (more than 70 entries in the ICSD database)[30], the same as that of the Re₇N₃ compound. We noticed that in Re₇N₃, the shortest and average distances between the Re–Re nearest neighbours (approximately 2.28 Å and 2.37 Å, respectively) are just slightly longer than the Re–Re distances in metallic rhenium (about 2.23 Å), which is present in the pressure chamber along with the nitride. A comparison of the shortest and average distances between the closest A–A neighbours in the Th₇Fe₃-type structured compounds with the metal–metal distances in corresponding pure metals at the same pressures (Extended Data Fig. 6) indeed shows a clear similarity. (In some cases—for example, in experimentally studied Fe₇C₃ at 158 GPa (ref. [31]), or theoretically predicted Fe₇N₃ at 150 GPa (ref. [32])—the A–A distances are even slightly shorter in compounds than pure metals). Notably, the average Re–N distance in NRe₆ prisms in Re₇N₃ (⟨Re–N⟩ is 1.84 Å) follows the same trend as for other Th₇Fe₃-type structured compounds when ⟨A–X⟩ is compared with ⟨A–A⟩ (Extended Data Fig. 6). According to our experimental data, the Re–N distances in trigonal prisms in Re₇N₃ vary from approximately 1.79 Å to 1.94 Å, as expected for pressures of several megabars (the shortest previously reported rhenium–nitrogen distance is approximately 1.96 Å in ReN₈·xN₂ at 134 GPa)[11]. We note that in the TPa pressure range, the Re–Re interatomic distances become comparable with those of transition metals of the fourth period (Cr, Mn, Fe, Ni), which are known to form Th₇Fe₃-type structured (or similar) compounds at ambient (or relatively low) pressure[30]. It may be an indication that a huge reduction of the Re size promotes formation of Re₇N₃ at several hundreds of GPa, but the existence of Ru₇B₃ at ambient pressure[30] (in ruthenium the metal–metal distance is approximately 2.68 Å versus approximately 2.75 Å in Re) suggests that the size factor may be important, but not necessarily crucial.

The synthesis of Re₇N₃ was reproduced in dsDAC #2. Diffraction data collected at ID11 at ESRF shows numerous diffraction spots, and the analysis of the integrated powder diffraction pattern confirmed the presence of the hexagonal phase with the lattice parameters very close to those obtained for Re₇N₃ in dsDAC #1 (Supplementary Tables 1, 3 and Extended Data Fig. 7). Unfortunately, the quality of the diffraction was insufficient for the single-crystal data analysis; the deterioration of the quality of diffraction data may be due to a pressure drop from around 140 GPa to 100 GPa on primary anvils upon laser-heating. Still, for dsDAC #2 we were able to release pressure to ambient without total destruction of the pressure chamber and found there a particle of almost 2 μm in diameter, which consisted of Re and N in the atomic ratio of about 2:1 (Extended Data Fig. 8). This finding provides additional evidence of the synthesis of rhenium nitride in dsDAC #2.

To elucidate the effect of the extreme compression on the stability of the Re₇N₃ compound and to characterize its physical properties, we carried out electronic structure calculations in the framework of density functional theory and studied its electronic, thermodynamic and vibrational properties (see Methods and Supplementary Information section 'Computational details'). The optimized lattice parameters and coordinates of atoms of Re₇N₃ were found to be in excellent agreement with experiment (Supplementary Table 4). A difference in pressure calculated at experimental volumes for Re₇N₃ may indicate that the calculated equation of state of Re

Article

and/or Re_7N_3 at ultrahigh compressions is becoming less accurate, which is often the case in generalized gradient approximation calculations. Examination of the electronic band structure (Supplementary Information section 'Electronic properties of Re_7N_3' and Supplementary Fig. 1), electronic density of states (Supplementary Figs. 2, 3), electron localization function (Supplementary Fig. 4), and charge density maps (Supplementary Fig. 5) show that Re_7N_3 is a metal that has a combination of metallic and ionic bonding with some covalent component.

The dsDAC #3 was laser-heated to a maximum temperature of 3,450(200) K and the lattice parameters of Re measured after heating were found to be $a = 2.2803(3)$ Å, $c = 3.622(1)$ Å and $V = 16.31(2)$ Å^3. According to the equation of state[27] of Re, the sample was under pressure of 730(4) GPa (Supplementary Table 1 and Supplementary Fig. 6). The analysis of single-crystal XRD data revealed the presence of a cubic phase (space group $Fm\overline{3}m$) with a lattice parameter of approximately 3.40 Å to approximately 3.41 Å depending on the spot from which the XRD pattern was taken. Structural solution suggests that the phase has an NaCl (B1)-type structure (Fig. 2 and Supplementary Fig. 7) with one position occupied by Re and the other by a light element. Attempts to refine the crystal structure assuming that the position of the light element is fully occupied by N or C led to an unreasonably high thermal parameter (approximately 0.1 Å^2). For the highly symmetric NaCl-type structure containing heavy Re atoms, simultaneous refinement of the occupancy and the thermal parameter of a lighter element is not reasonable, so we constrained the thermal parameters of all atoms to be equal. In this approximation, the composition of the cubic phase was $ReN_{0.20}$ (Supplementary Table 2). Of course, on the basis of XRD data alone we could not exclude that the light element might be carbon, but theoretical calculations (see Supplementary Information section 'Re-based solution phase') suggest that nitrogen is more plausible. A partial occupation of octahedral voids of the underlying face-centred cubic (fcc) packing of Re atoms by nitrogen predicts negative formation enthalpies of metastable alloys (Supplementary Figs. 8, 9 and Supplementary Table 5), whereas filling them with carbon leads to positive formation enthalpies (Supplementary Fig. 8 and Supplementary Table 6).

Theoretical simulations enabled an insight into the possibility of synthesizing Re_7N_3 at pressures lower than those achieved in the current study. At 100 GPa the formation enthalpy of metastable Re_7N_3 is well above the convex hull (Fig. 3, Supplementary Information section 'Thermodynamic stability of Re_7N_3' and Extended Data Fig. 9). Even taking into account the anomalously large (approximately 0.2 eV per atom) metastability range of nitrides[33], this compound cannot be considered as synthesizable at 100 GPa. By contrast, at 730 GPa the calculated formation enthalpy of Re_7N_3, although still above the convex hull, becomes well within the metastability range of nitrides (Fig 3, Supplementary Information section 'Lattice dynamics of Re_7N_3' and Extended Data Fig. 9), and at approximately 900 GPa—the pressure of the realized experimental synthesis—it lies on the convex hull (Fig. 3).

Pressures of more than several megabars have long been thought to have a profound effect on the chemistry and physics of materials[1,2] and to lead to formation of phases with exotic crystal structures. In this work we have demonstrated that at pressures as high as those exceeding 600 GPa new compounds can be synthesized in laser-heated dsDACs and their structures can be solved in situ. By extending the experimental field of high-pressure synthesis and structural studies to the terapascal range, our work paves the way towards the discovery of new materials and observations of novel physical phenomena.

Online content

Any methods, additional references, Nature Research reporting summaries, source data, extended data, supplementary information, acknowledgements, peer review information; details of author contributions and competing interests; and statements of data and code availability are available at https://doi.org/10.1038/s41586-022-04550-2.

1. McMillan, P. F. Chemistry at high pressure. *Chem. Soc. Rev.* **35**, 855–857 (2006).
2. Needs, R. J. & Pickard, C. J. Role of structure prediction in materials discovery and design. *APL Mater.* **4**, 053210 (2016).
3. Dubrovinsky, L., Dubrovinskaia, N., Prakapenka, V. B. & Abakumov, A. M. Implementation of micro-ball nanodiamond anvils for high-pressure studies above 6 Mbar. *Nat. Commun.* **3**, 1163 (2012).
4. Austin, I. G. & Mott, N. F. Metallic and nonmetallic behavior in transition metal oxides: electron correlation effects in narrow *d* bands and polarons are discussed. *Science* **168**, 71–77 (1970).
5. Shimizu, K. et al. Superconductivity in the non-magnetic state of iron under pressure. *Nature* **412**, 316–318 (2001).
6. Kim, E. & Chan, M. H. W. Probable observation of a supersolid helium phase. *Nature* **427**, 225–227 (2004).
7. Dewaele, A., Loubeyre, P., Occelli, F., Marie, O. & Mezouar, M. Toroidal diamond anvil cell for detailed measurements under extreme static pressures. *Nat. Commun.* **9**, 2913 (2018).
8. Jenei, Z. et al. Single crystal toroidal diamond anvils for high pressure experiments beyond 5 megabar. *Nat. Commun.* **9**, 3563 (2018).
9. Laniel, D. et al. High-pressure polymeric nitrogen allotrope with the black phosphorus structure. *Phys. Rev. Lett.* **124**, 216001 (2020).
10. Friedrich, A. et al. Novel rhenium nitrides. *Phys. Rev. Lett.* **105**, 085504 (2010).
11. Bykov, M. et al. High-pressure synthesis of a nitrogen-rich inclusion compound $ReN_8 \cdot xN_2$ with conjugated polymeric nitrogen chains. *Angew. Chem. Int. Ed.* **57**, 9048–9053 (2018).
12. Bykov, M. et al. Synthesis of FeN_4 at 180 GPa and its crystal structure from a submicron-sized grain. *Acta Crystallogr. E* **74**, 1392–1395 (2018).
13. Bykov, M. et al. High-pressure synthesis of ultraincompressible hard rhenium nitride pernitride $Re_2(N_2)(N)_2$ stable at ambient conditions. *Nat. Commun.* **10**, 2994 (2019).
14. Bykov, M. et al. Synthesis of arsenopyrite-type rhodium pernitride RhN_2 from a single-source azide precursor. *Eur. J. Inorg. Chem.* **2019**, 3667–3671 (2019).
15. Bykov, M. et al. High-pressure synthesis of metal–inorganic frameworks $Hf_4N_{20} \cdot N_2$, $WN_8 \cdot N_2$, and $Os_5N_{23} \cdot N_2$ with polymeric nitrogen linkers. *Angew. Chem. Int. Ed.* **59**, 10321–10326 (2020).
16. Khandarkhaeva, S. et al. Novel rhenium carbides at 200 GPa. *Eur. J. Inorg. Chem.* **2020**, 2186–2190 (2020).
17. Dubrovinskaia, N. et al. Terapascal static pressure generation with ultrahigh yield strength nanodiamond. *Sci. Adv.* **2**, e1600341 (2016).
18. Dubrovinsky, L. et al. The most incompressible metal osmium at static pressures above 750 gigapascals. *Nature* **525**, 226–229 (2015).
19. Bykova, E. *Single-Crystal X-Ray Diffraction at Extreme Conditions in Mineral Physics and Material Sciences*. PhD thesis, Univ. Bayreuth (2015).
20. Dubrovinskaia, N. & Dubrovinsky, L. Crystallography taken to the extreme. *Phys. Scr.* **93**, 062501 (2018).
21. Kantor, I. et al. BX90: a new diamond anvil cell design for X-ray diffraction and optical measurements. *Rev. Sci. Instrum.* **83**, 125102 (2012).
22. Kurnosov, A. et al. A novel gas-loading system for mechanically closing of various types of diamond anvil cells. *Rev. Sci. Instrum.* **79**, 045110 (2008).
23. Akahama, Y., Hirao, N., Ohishi, Y. & Singh, A. K. Equation of state of bcc-Mo by static volume compression to 410 GPa. *J. Appl. Phys.* **116**, 223504 (2014).
24. Akahama, Y. & Kawamura, H. Pressure calibration of diamond anvil Raman gauge to 410 GPa. *J. Phys. Conf. Ser.* **215**, 012195 (2010).
25. Aprilis, G. et al. Portable double-sided pulsed laser heating system for time-resolved geoscience and materials science applications. *Rev. Sci. Instrum.* **88**, 084501 (2017).
26. Fedotenko, T. et al. Laser heating setup for diamond anvil cells for in situ synchrotron and in house high and ultra-high pressure studies. *Rev. Sci. Instrum.* **90**, 104501 (2019).
27. Anzellini, S., Dewaele, A., Occelli, F., Loubeyre, P. & Mezouar, M. Equation of state of rhenium and application for ultra high pressure calibration. *J. Appl. Phys.* **115**, 043511 (2014).
28. Sakai, T. et al. High pressure generation using double-stage diamond anvil technique: problems and equations of state of rhenium. *High Press. Res.* **38**, 107–119 (2018).
29. Li, W.-K., Zhou, G.-D. & Mak, T. *Advanced Structural Inorganic Chemistry* (Oxford Univ. Press, 2008).
30. ICSD database; https://icsd.products.fiz-karlsruhe.de
31. Prescher, C. et al. High Poisson's ratio of Earth's inner core explained by carbon alloying. *Nat. Geosci.* **8**, 220–223 (2015).
32. Sagatov, N., Gavryushkin, P. N., Inerbaev, T. M. & Litasov, K. D. New high-pressure phases of Fe_7N_3 and Fe_7C_3 stable at Earth's core conditions: evidence for carbon–nitrogen isomorphism in Fe-compounds. *RSC Adv.* **9**, 3577–3581 (2019).
33. Sun, W. et al. The thermodynamic scale of inorganic crystalline metastability. *Sci. Adv.* **2**, e1600225 (2016).
34. Zhao, Z. et al. Nitrogen concentration driving the hardness of rhenium nitrides. *Sci Rep.* **4**, 4797 (2015).

Methods

Diffraction data were acquired at ID11 beamline at ESRF. Experiments with dsDAC #1 were performed using a Frelon 4M detector, wavelength 0.3099 Å, beam size 0.45 × 0.45 μm^2 at FWHM; data for dsDAC #2 and dsDAC #3 were collected with Eiger2 CdTe 4M detector, wavelength 0.2882 Å, beam size 0.5 × 0.5 μm^2 at FWHM. 2D mappings of still XRD images (without ω oscillations) were performed with an exposure time up to 10 s; single-crystal datasets were collected via DACs rotation around the ω axis from −38° to 38° with an angular step of 0.5° and an acquisition time of 10 s per step.

For the powder diffraction studies, calibration of instrument model and integration of diffraction patterns were made in the DIOPTAS[35] software using CeO$_2$ powder standard (NIST SRM 674b). Integrated patterns from powder XRD experiments were processed using the Le Bail technique implemented in JANA2006[36] software. XRD imaging of the sample chamber was reconstructed using XDI[37] programme and map of still images converted from 'edf' to 'tif' format. For the single-crystal XRD, integration of the reflection intensities and absorption corrections were performed in CrysAlisPro software[38]. A single crystal of orthoenstatite (Mg$_{1.93}$,Fe$_{0.06}$)(Si$_{1.93}$,Al$_{0.06}$)O$_6$ (space group $Pbca$, a = 8.8117(2) Å, b = 5.18320(10) Å, c = 18.2391(3) Å) was used as calibration standard for refinement of the instrument model of the diffractometer. Diffraction images were converted from 'edf' to the native CrysAlisPro format 'ESPERANTO' with Freac software[38]. Detailed information of integration parameters as well as of the data-reduction output files and indicators of the XRD data quality are given in ref. [19]. The crystal structures were solved using SHELXT or the superflip method in JANA2006 and Olex2[36,39,40]. Crystal structures were refined by least-squares minimization of adjustable parameters. We performed isotropic refinement of atomic displacement parameters due to limited dataset collected in DAC. Reflections coming from parasite diffraction produced by diamonds and crystallized pressure media were eliminated during the refinement procedure. The software Diamond[41] was used for visualization of molecular graphics.

The electronic structure, total energy and forces calculations of the studied rhenium nitrides were carried out in the framework of density functional theory (see Supplementary Information section 'Computational details'). We used supercells of different sizes with an underlying fcc crystal structure and various amounts of either N or C to simulate the Re–N and Re–C cubic phases with NaCl (B1)-type structure (see Supplementary Information section 'Re-based solution phase'). To investigate the influence of pressure on the thermodynamic stability of Re$_7$N$_3$, its enthalpy of formation, as well as the enthalpies of formation for various phases of rhenium nitride, known experimentally[10,11,13] and predicted theoretically[34], were calculated and a thermodynamic convex hull was constructed based on the calculation results (Supplementary Information section 'Thermodynamic stability of Re$_7$N$_3$').

Phonon dispersion relations for Re$_7$N$_3$ were calculated in the harmonic approximation at volume 200 Å^3 (a = 7.122 Å, c = 4.553 Å) of the unit cell, corresponding to P = 102 GPa, as well as at experimental volume 136.52 Å^3 (a = 6.277 Å, c = 4.001 Å) of the unit cell (Supplementary Table 4), which corresponded to calculated pressure 732 GPa (see Extended Data Fig. 9 and Supplementary Information section 'Computational details'). Because Re$_7$N$_3$ is predicted to be dynamically unstable at the synthesis pressure owing to the presence of imaginary frequencies in this approximation (Extended Data Fig. 9 and Supplementary Information section 'Lattice dynamics of Re$_7$N$_3$'), we investigated the anharmonic effects of lattice vibrations at finite temperature using the temperature-dependent effective potential (TDEP) method[42] with effective second-order and third-order interatomic force constants calculated from first principles[43]. The calculations are based on modelling the potential energy surface in the vicinity of equilibrium with a Hamiltonian of the form:

$$H = U_0 + \sum_i \frac{\mathbf{p}_i^2}{2m_i} + \frac{1}{2!} \sum_{ij\alpha\beta} \Phi_{ij}^{\alpha\beta} u_i^\alpha u_j^\beta + \frac{1}{3!} \sum_{ijk\alpha\beta\gamma} \Phi_{ijk}^{\alpha\beta\gamma} u_i^\alpha u_j^\beta u_k^\gamma + \dots, \quad (1)$$

where $\mathbf{p}$ and m are the momentum and the mass of ion i, respectively, Φ are interaction parameters (the effective force constants) of increasing order, u denotes the displacement of ions (i, j or k) from their equilibrium positions, and $\alpha\beta\gamma$ are Cartesian components.

We calculated the spectral function $S(\mathbf{q}, E)$ at 300 K, which describes the spectrum of lattice excitations with energy $E = \hbar\Omega$ (Ω is the applied frequency) for mode s with harmonic frequency $\omega_{\mathbf{q}s}$ at wavevector $\mathbf{q}$ (refs. [44,45]). $S(\mathbf{q}, E)$ provides insight into the phonon frequencies as well as strength of three-phonon processes via the broadening in Extended Data Fig. 9. The $S(\mathbf{q}, E)$ of Re$_7$N$_3$ is typical of a weakly anharmonic solid with Lorentzian broadening of single peaks. Additionally, the lines are reasonably crisp, without substantial broadening, indicating that the anharmonic interaction strength is well within the range of validity for the perturbation theory. Importantly, Re$_7$N$_3$ is seen to be dynamically stable (there are no imaginary frequencies) at the synthesis pressure (see Supplementary Information section 'Lattice dynamics of Re$_7$N$_3$').

Reporting summary

Further information on research design is available in the Nature Research Reporting Summary linked to this paper.

Data availability

Data supporting this work are available at Zenodo, https://doi.org/10.5281/zenodo.5899162. Structural data deposit at Cambridge Crystallographic Data Centre (CCDC), CSD-2143754 (https://doi.org/10.25505/fiz.icsd.cc29yrcd).

Code availability

The temperature-dependent effective potential method is implemented as a package that deals with finite-temperature lattice dynamics in solids. The package is released under the MIT license, available on GitHub, see https://ollehellman.github.io. Source files for TDEP 1.1 are located at https://ollehellman.github.io/lists/files.html.

35. Prescher, C. & Prakapenka, V. B. DIOPTAS: a program for reduction of two-dimensional X-ray diffraction data and data exploration. *High Press. Res.* **35**, 223–230 (2015).
36. Petříček, V., Dušek, M. & Palatinus, L. Crystallographic computing system JANA2006: general features. *Z. Kristallogr. Cryst. Mater.* **229**, 345–352 (2014).
37. Hrubiak, R., Smith, J. S. & Shen, G. Multimode scanning X-ray diffraction microscopy for diamond anvil cell experiments. *Rev. Sci. Instrum.* **90**, 025109 (2019).
38. CrysAlis Pro v. 171.40.84 (Rigaku, 2020).
39. Sheldrick, G. M. SHELXT – integrated space-group and crystal-structure determination. *Acta Crystallogr. A* **71**, 3–8 (2015).
40. Dolomanov, O. V., Bourhis, L. J., Gildea, R. J., Howard, J. A. K. & Puschmann, H. OLEX2: a complete structure solution, refinement and analysis program. *J. Appl. Crystallogr.* **42**, 339–341 (2009).
41. Putz, H. & Brandenburg, K. Diamond – Crystal and Molecular Structure Visualization Version 4 (Crystal Impact, 2021).
42. Hellman, O., Abrikosov, I. A. & Simak, S. I. Lattice dynamics of anharmonic solids from first principles. *Phys. Rev. B* **84**, 180301 (2011).
43. Hellman, O. & Abrikosov, I. A. Temperature-dependent effective third-order interatomic force constants from first principles. *Phys. Rev. B* **88**, 144301 (2013).
44. Cowley, R. A. Anharmonic crystals. *Rep. Prog. Phys.* **31**, 123–166 (1968).
45. Maradudin, A. A. & Fein, A. E. Scattering of neutrons by an anharmonic crystal. *Phys. Rev.* **128**, 2589–2608 (1962).

Article

a

b

c

d

e

Extended Data Fig. 1 | Toroidal profile produced by FIB milling on a culet of a conventional anvil. a, Original Boehler–Almax-type single-bevelled diamond anvils with 40-µm culets (before milling). **b**, Greyscale bitmap used for milling. **c**, The milling depth profile. **d**, Crafted toroidal culet. **e**, Cross-sectional schematic of the dsDAC assembly (not to scale): a gasket (grey) with the pressure chamber (dark grey; the sample is yellow) squeezed between the two toroidal diamond anvils (light blue) equipped with hemispheres of nanocrystalline diamond (white); the pressure chamber is of 6 µm in diameter and 4 µm in height. The gasket was prepared as follows: We used strips of a 200-µm thick Re foil. To make an indentation with a thickness of about 4 µm, we followed a many-step procedure. First, the Re foil was pre-indented to a thickness of ~20 µm using a pair of single-bevelled diamonds with 80-µm culets. Then, a hole about 30 µm in diameter was laser-drilled in the centre of the indentation, and the indentation was pressurized again between the same bevelled diamonds. This led to closing of the hole and a reduction in the thickness of the indentation. This procedure was repeated a few times until a thickness of about 7 µm was achieved. The gasket was mounted into a BX-90 DAC equipped with toroidal diamond anvil and indented by their miniature 10-µm culets to a thickness of ~4 µm. A hole (~6 µm in diameter) in the centre of the ~10-µm indentation was made using FIB or by tightly focused pulsed near-infrared laser to form a pressure chamber.
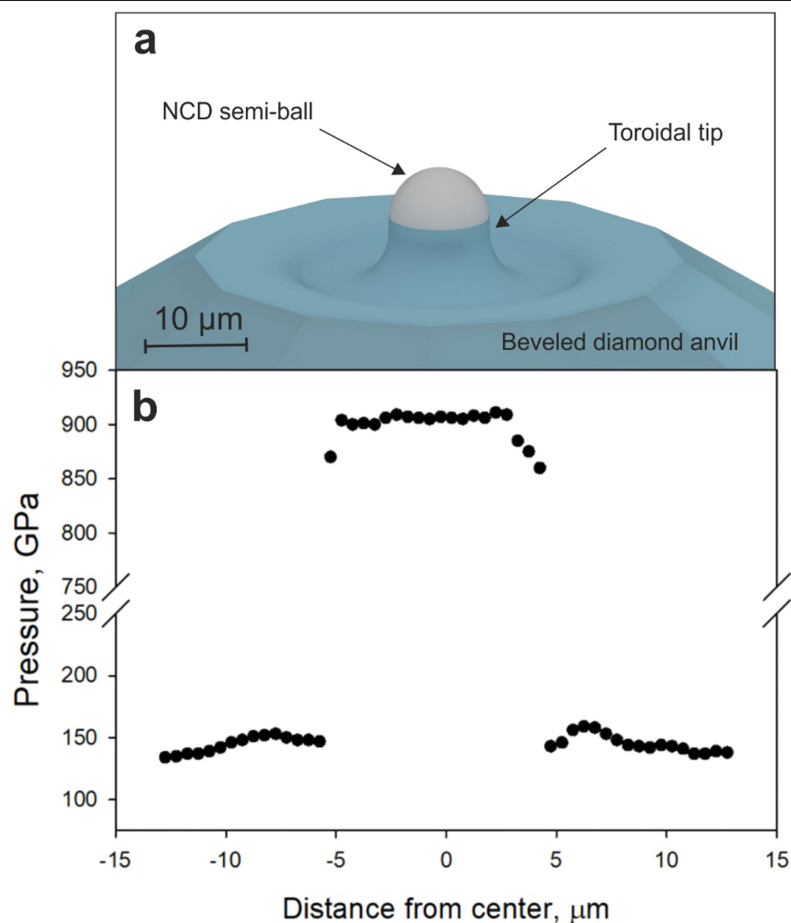
Extended Data Fig. 2 | A schematic illustration of the experimental set-up. a, Three-dimensional presentation of a diamond anvil featuring a toroidal profile milled by FIB on the surface of a conventional Boehler–Almax-type single-bevelled diamond anvil with a 40-µm culet. A hemisphere of transparent nanocrystalline diamond (NCD)[17], which was FIB-milled from a single ball with a diameter of 12 to 14 µm, was placed over the tip to realize a double-stage DAC design. Two anvils of this kind were forced together as shown in the scheme in Extended Data Fig. 1. **b**, Pressure profile along the cross-section through the centre of dsDAC #1 after pulsed laser-heating. Diffraction patterns were collected at each point with a step of 0.5 µm at the ID11 beamline at ESRF, and pressure was determined according to the equation of state from ref. [27] using the lattice parameters of Re found from powder diffraction data.
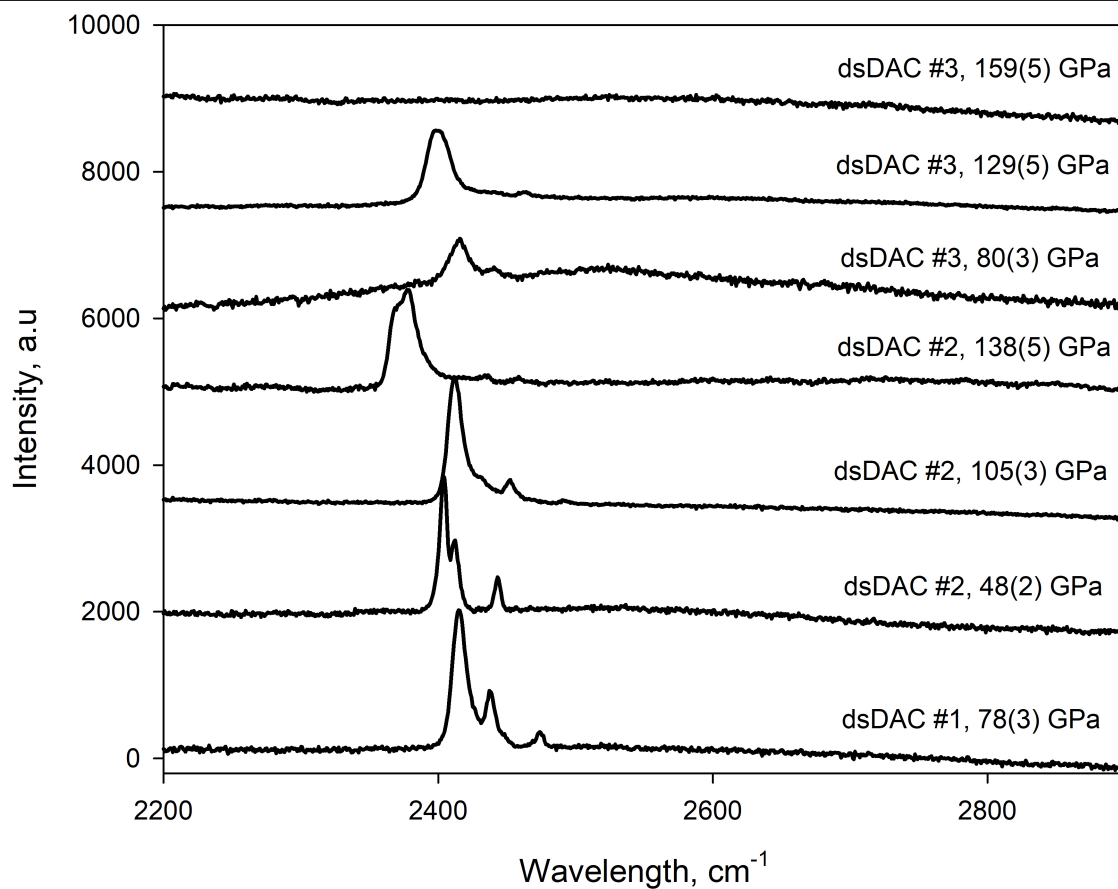
Extended Data Fig. 3 | Raman spectra taken upon compression of the dsDAC after nitrogen gas loading featuring nitrogen vibron. At pressures above ~160 GPa the Raman signal of nitrogen becomes non-detectable. The pressures were determined according to ref. [24]. a.u., arbitrary units.
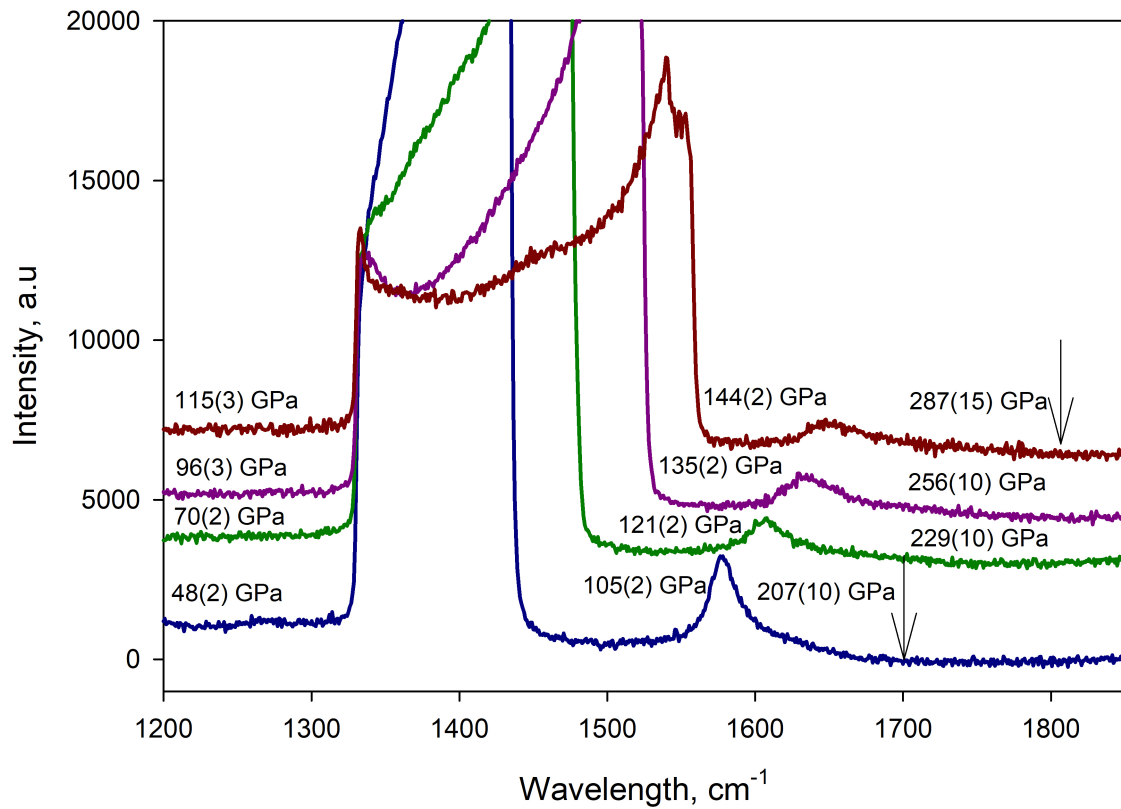
Extended Data Fig. 4 | The evolution of Raman spectra of primary and secondary anvils upon compression of dsDAC #2. The pressure is determined from diamond line Raman shift[24]. The pressures on primary anvil are shown on the left. The peaks at ~1,600 cm^{-1} are the pressures on the body of the secondary anvil. The values on the right give estimates of pressures from the broadened Raman line of the secondary anvil (the arrows provide examples of positions found by analysis of the first derivatives of the spectra). Reliable determination of the pressure in the chamber from the Raman shift of the diamond line of the secondary nanocrystalline diamond anvils is not feasible.
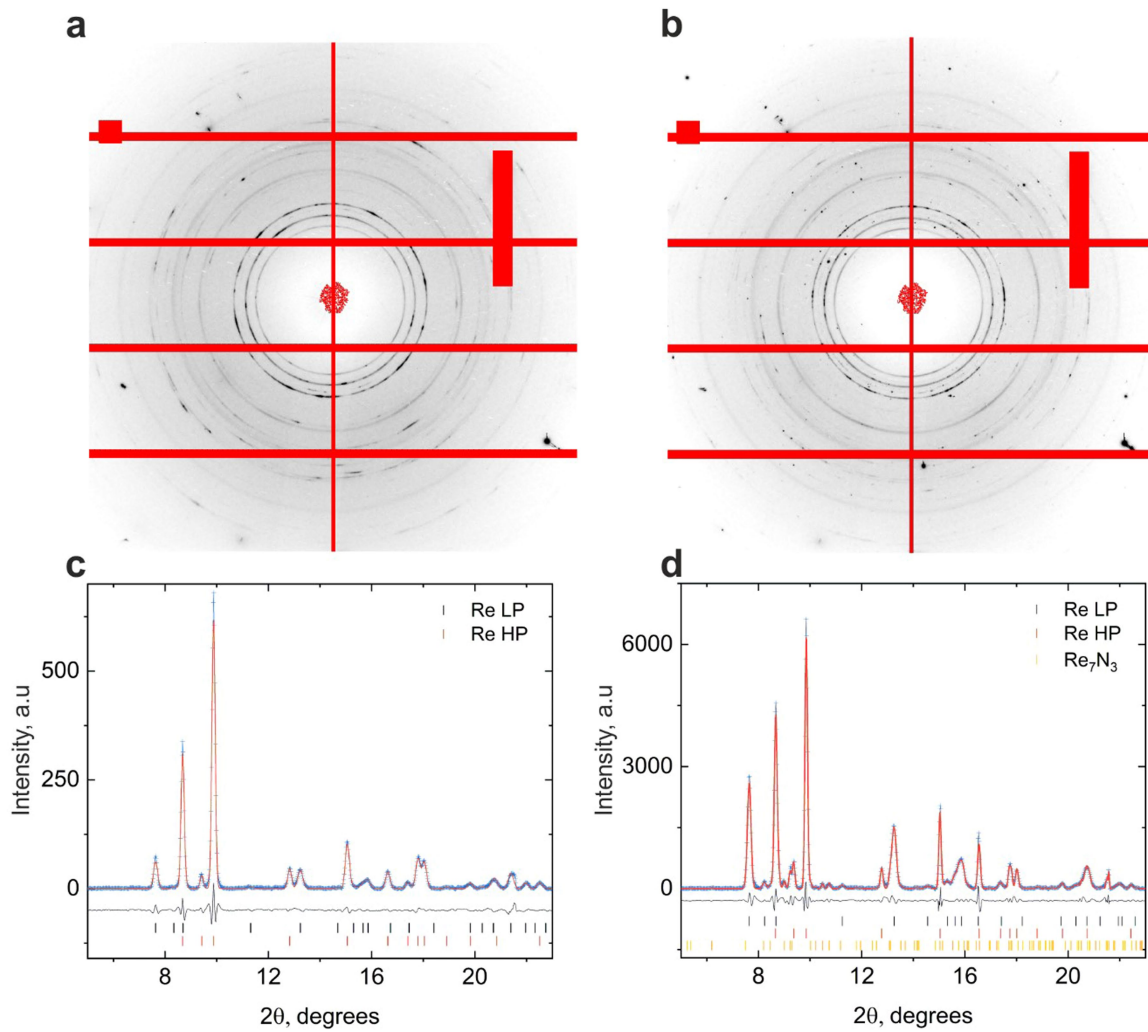
Extended Data Fig. 5 | Examples of powder diffraction patterns collected from dsDAC #1. Data collected at 13-IDD (Advanced Photon Source, USA; beam FWHM, 3×3 μm²). **a**, The centre of the pressure chamber of the as-compressed ds-DAC. **c**, Re LP (low pressure): $a = 2.5606(5)$ Å, $c = 4.0588(12)$ Å and $V = 23.047(7)$ Å³, that is, 149(3) GPa according to the equation of state from ref. [27], or 173(3) GPa according to ref. [3]; Re HP (high pressure): $a = 2.2214(3)$ Å, $c = 3.5609(8)$ Å and $V = 15.21(1)$ Å³, that is, 930(5) GPa[27] or 1298(10) GPa[3].

b, After pulsed laser-heating at 2,200(200) K during 5 s. **d**, Re LP: $a = 2.5577(3)$ Å, $c = 4.1095(12)$ Å and $V = 23.282(7)$ Å³, at 140(3) GPa[27] or 162(3) GPa[3]; Re HP: $a = 2.2297(2)$ Å, $c = 3.5735(5)$ Å and $V = 15.38(1)$ Å³, at 895(5) GPa[27] or 1,250(10) GPa[3]; Re₇N₃: $a = 6.3086(4)$ Å, $c = 4.0048(7)$ Å and $V = 138.04(4)$ Å³. Structural data for Re_7N_3 were taken from the results of single-crystal XRD data analysis.

a

b

c
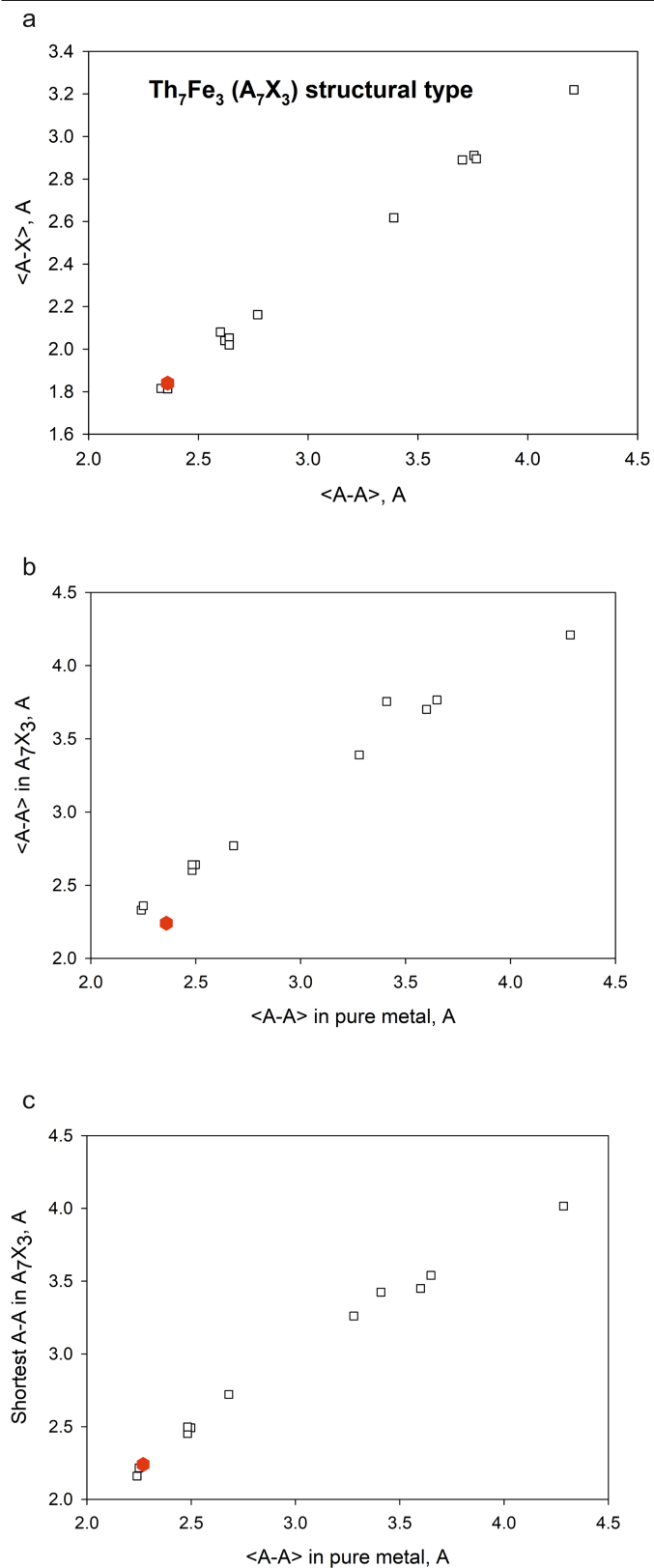
Extended Data Fig. 6 | Interatomic distances in Th$_7$Fe$_3$ structured and some other selected A_7X_3 compounds. a, **b**, Comparison of shortest (**a**) and average between first neighbours (**b**) A–A distances in A_7X_3 compounds with metal–metal contacts in corresponding pure metals (A) at the same pressures. **c**, Correlation between average $\langle X$–$A \rangle$ distances in XA_6 prisms and first neighbours $\langle A$–$A \rangle$ distances. The red hexagons correspond to Re$_7$N$_3$ as described in this work; data for orthorhombic Fe$_7$C$_3$ at 158 GPa are from ref. [35], data for predicted Fe$_7$N$_3$ at 150 GPa are from ref. [32], all other data are from ref. [30].

a

Re$_7$N$_3$

Re HP (1 0 1)

Re HP (0 0 2)

Diamond

b

Exp. data
Le Bail fit
Difference
Re$_7$N$_3$
Re HP
Re LP

Intensity, a. u.

Re$_7$N$_3$ (1 0 1)
Re$_7$N$_3$ (2 0 0)
Re HP (0 0 2)
Re$_7$N$_3$ (3 -1 1)
Re HP (1 0 1)
Re$_7$N$_3$ (2 -1 2)
Re$_7$N$_3$ (3 0 1)
Re$_7$N$_3$ (5 -2 0)
Re HP (2 -1 0)
Re$_7$N$_3$ (6 -2 2)

2θ, degrees
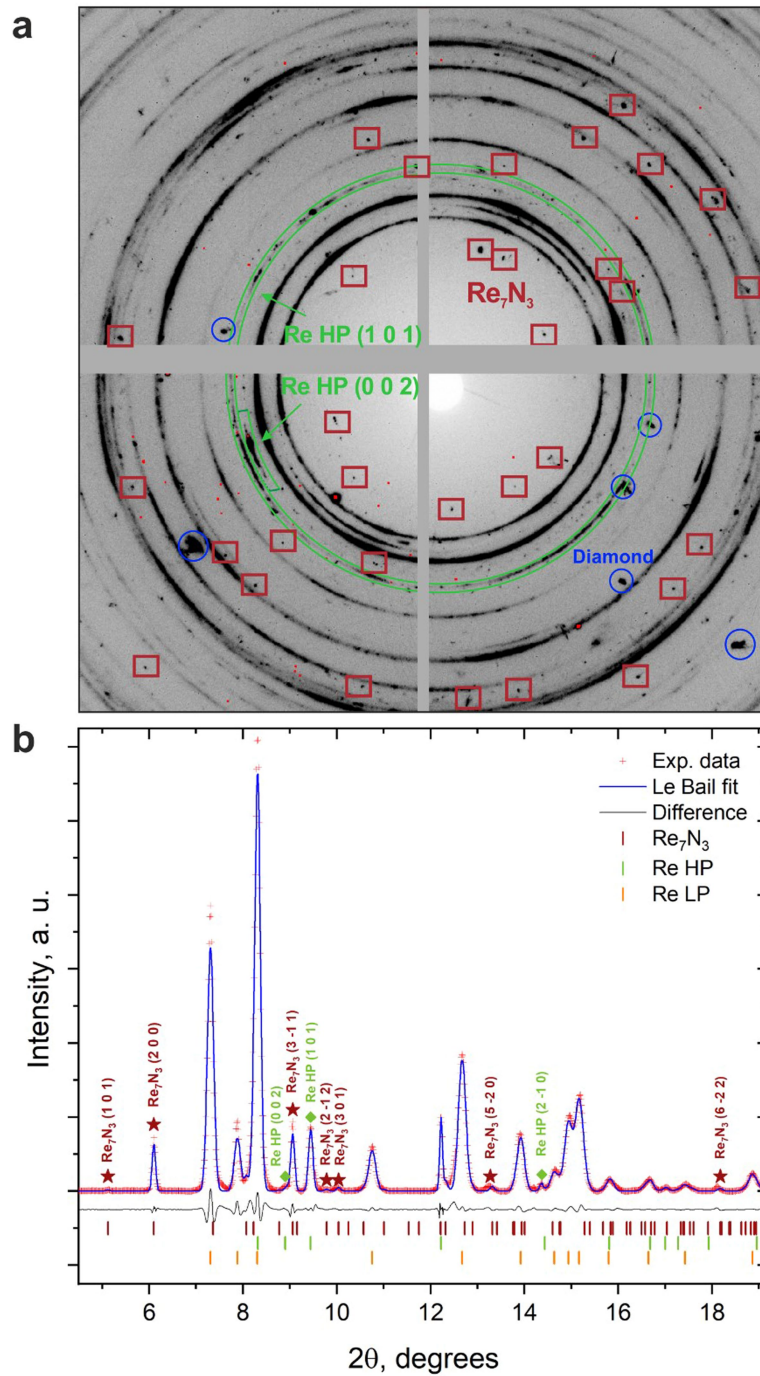
Extended Data Fig. 7 | Example of powder diffraction pattern collected from dsDAC #2. Data were collected at ID11 (ESRF, Grenoble, France, beam FWHM 0.5 × 0.5 μm²) at 646 GPa (see Supplementary Table 1). **a**, 2D diffraction image shows diffraction spots of Re$_7$N$_3$ and rings of hexagonal close-packed (hcp) Re at different pressures. **b**, Refinement of powder diffraction pattern with Le Bail fit implemented in JANA2006 software. The values of the lattice parameters are given in Supplementary Table 3.

a

| 1 μm | EHT = 20.00 kV | Signal A = SE2 | Date :23 Jun 2021 | ZEISS |
| | WD = 14.2 mm | Photo No. = 27204 | Mag = 12.65 K X | |
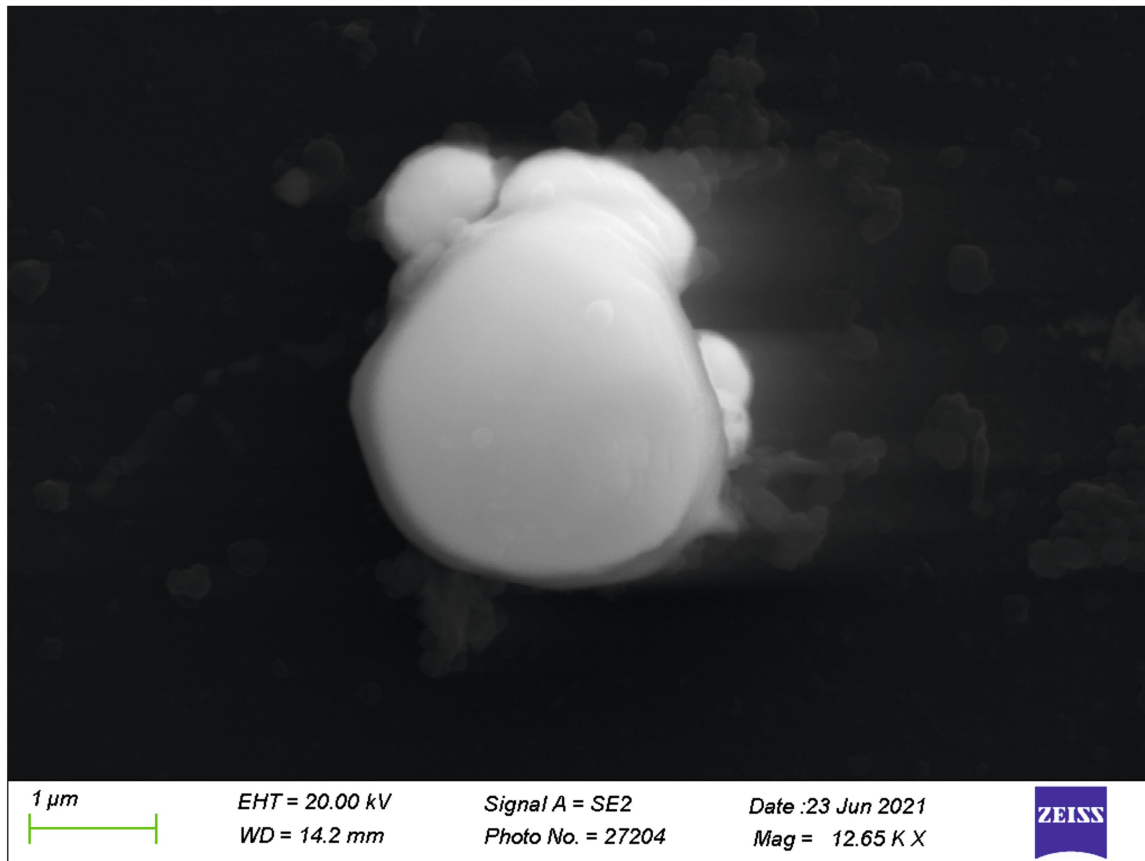
b
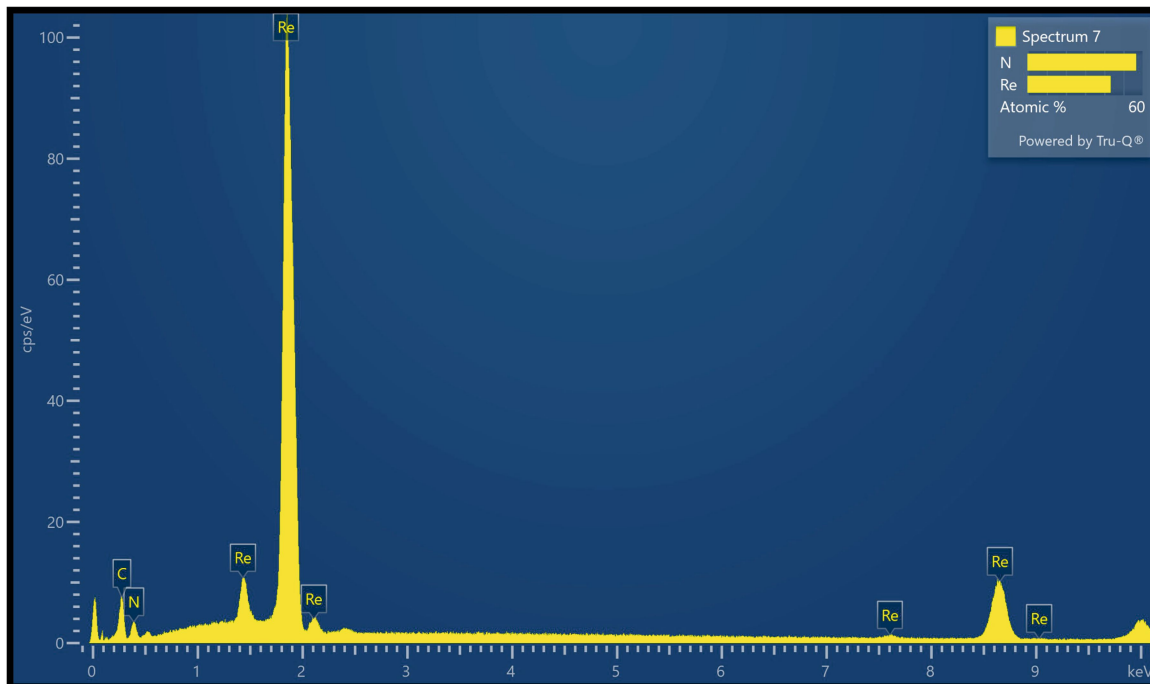
Extended Data Fig. 8 | Characteristics of a sample extracted from the dsDAC #2. Sample contains Re and N in atomic proportions ~2:1. **a**, SEM image; **b**, example of EDX spectra. Images and spectra were collected on a ZEISS SEM, Leo Gemini 1530 with a Schottky field emission gun employing an accelerating voltage of 20 kV.
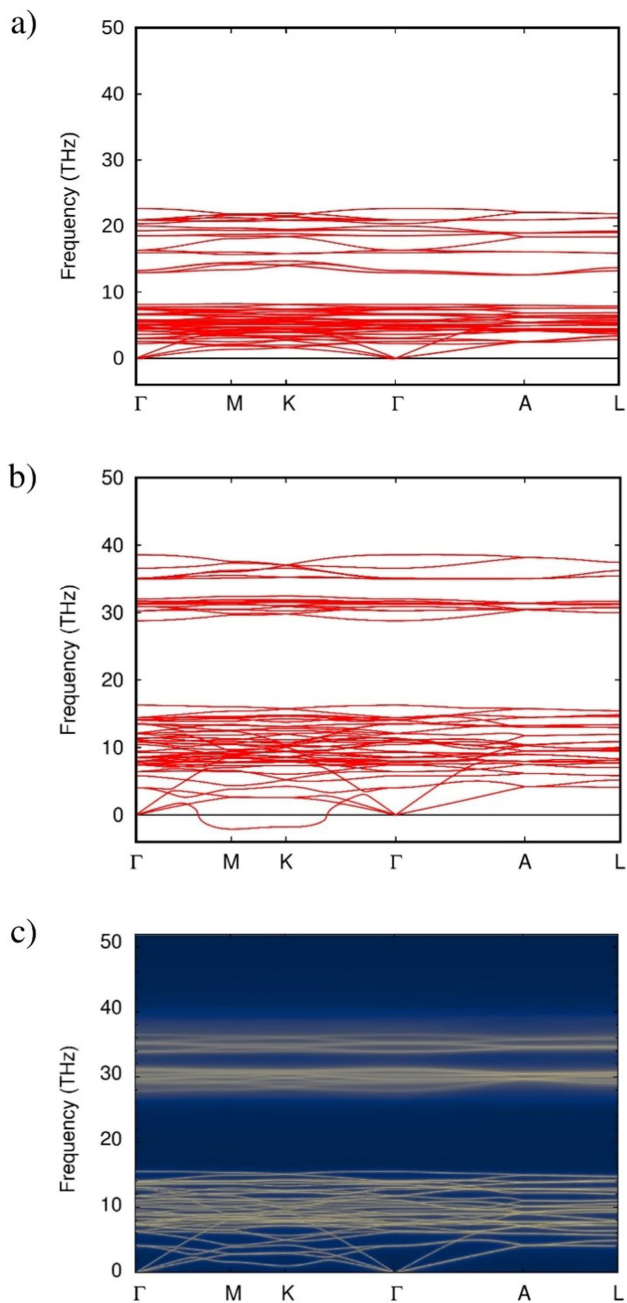
Extended Data Fig. 9 | Phonon dispersion relations for Re_7N_3 calculated within the harmonic approximation. a, Theoretical pressure $P = 102$ GPa. **b**, Experimental volume 136.52 Å^3, which corresponds to theoretical pressure -730 GPa. **c**, Vibrational spectral function at $P \approx 730$ GPa and $T = 300$ K, calculated using the temperature-dependent effective potential (TDEP) method. The results show that in the harmonic approximation, Re_7N_3 is unstable at the synthesis pressure (imaginary frequencies are shown below the zero-frequency line). Including anharmonic effects of lattice vibrations removes the dynamical instability at $P = 730$ GPa (all the branches are real).

nature portfolio

Corresponding author(s): Dubrovinsky

Last updated by author(s): Jan 25, 2022

Reporting Summary

Nature Portfolio wishes to improve the reproducibility of the work that we publish. This form provides structure for consistency and transparency in reporting. For further information on Nature Portfolio policies, see our Editorial Policies and the Editorial Policy Checklist.

Statistics

For all statistical analyses, confirm that the following items are present in the figure legend, table legend, main text, or Methods section.

n/a	Confirmed	
☐	☒	The exact sample size (*n*) for each experimental group/condition, given as a discrete number and unit of measurement
☐	☒	A statement on whether measurements were taken from distinct samples or whether the same sample was measured repeatedly
☐	☒	The statistical test(s) used AND whether they are one- or two-sided *Only common tests should be described solely by name; describe more complex techniques in the Methods section.*
☒	☐	A description of all covariates tested
☐	☒	A description of any assumptions or corrections, such as tests of normality and adjustment for multiple comparisons
☐	☒	A full description of the statistical parameters including central tendency (e.g. means) or other basic estimates (e.g. regression coefficient) AND variation (e.g. standard deviation) or associated estimates of uncertainty (e.g. confidence intervals)
☒	☐	For null hypothesis testing, the test statistic (e.g. *F*, *t*, *r*) with confidence intervals, effect sizes, degrees of freedom and *P* value noted *Give P values as exact values whenever suitable.*
☒	☐	For Bayesian analysis, information on the choice of priors and Markov chain Monte Carlo settings
☒	☐	For hierarchical and complex designs, identification of the appropriate level for tests and full reporting of outcomes
☒	☐	Estimates of effect sizes (e.g. Cohen's *d*, Pearson's *r*), indicating how they were calculated

Our web collection on statistics for biologists contains articles on many of the points above.

Software and code

Policy information about availability of computer code

Data collection	Standard software at ID11 (ESRF) and IDD-13 (APS) beam-lines
Data analysis	Commercially available CrysAlisPro v. 41 crystallographic software

For manuscripts utilizing custom algorithms or software that are central to the research but not yet described in published literature, software must be made available to editors and reviewers. We strongly encourage code deposition in a community repository (e.g. GitHub). See the Nature Portfolio guidelines for submitting code & software for further information.

Data

Policy information about availability of data

All manuscripts must include a data availability statement. This statement should provide the following information, where applicable:
- Accession codes, unique identifiers, or web links for publicly available datasets
- A description of any restrictions on data availability
- For clinical datasets or third party data, please ensure that the statement adheres to our policy

Data supporting this work are available at Zenodo, DOI: 105281/zenodo.5899162. Structural data deposit at Cambridge Crystallographic Data Centre (CCDC), CSD-2143754.

Field-specific reporting

Please select the one below that is the best fit for your research. If you are not sure, read the appropriate sections before making your selection.

☐ Life sciences   ☐ Behavioural & social sciences   ☐ Ecological, evolutionary & environmental sciences

For a reference copy of the document with all sections, see nature.com/documents/nr-reporting-summary-flat.pdf

Life sciences study design

All studies must disclose on these points even when the disclosure is negative.

Sample size	Describe how sample size was determined, detailing any statistical methods used to predetermine sample size OR if no sample-size calculation was performed, describe how sample sizes were chosen and provide a rationale for why these sample sizes are sufficient.
Data exclusions	Describe any data exclusions. If no data were excluded from the analyses, state so OR if data were excluded, describe the exclusions and the rationale behind them, indicating whether exclusion criteria were pre-established.
Replication	Describe the measures taken to verify the reproducibility of the experimental findings. If all attempts at replication were successful, confirm this OR if there are any findings that were not replicated or cannot be reproduced, note this and describe why.
Randomization	Describe how samples/organisms/participants were allocated into experimental groups. If allocation was not random, describe how covariates were controlled OR if this is not relevant to your study, explain why.
Blinding	Describe whether the investigators were blinded to group allocation during data collection and/or analysis. If blinding was not possible, describe why OR explain why blinding was not relevant to your study.

Behavioural & social sciences study design

All studies must disclose on these points even when the disclosure is negative.

Study description	Briefly describe the study type including whether data are quantitative, qualitative, or mixed-methods (e.g. qualitative cross-sectional, quantitative experimental, mixed-methods case study).
Research sample	State the research sample (e.g. Harvard university undergraduates, villagers in rural India) and provide relevant demographic information (e.g. age, sex) and indicate whether the sample is representative. Provide a rationale for the study sample chosen. For studies involving existing datasets, please describe the dataset and source.
Sampling strategy	Describe the sampling procedure (e.g. random, snowball, stratified, convenience). Describe the statistical methods that were used to predetermine sample size OR if no sample-size calculation was performed, describe how sample sizes were chosen and provide a rationale for why these sample sizes are sufficient. For qualitative data, please indicate whether data saturation was considered, and what criteria were used to decide that no further sampling was needed.
Data collection	Provide details about the data collection procedure, including the instruments or devices used to record the data (e.g. pen and paper, computer, eye tracker, video or audio equipment) whether anyone was present besides the participant(s) and the researcher, and whether the researcher was blind to experimental condition and/or the study hypothesis during data collection.
Timing	Indicate the start and stop dates of data collection. If there is a gap between collection periods, state the dates for each sample cohort.
Data exclusions	If no data were excluded from the analyses, state so OR if data were excluded, provide the exact number of exclusions and the rationale behind them, indicating whether exclusion criteria were pre-established.
Non-participation	State how many participants dropped out/declined participation and the reason(s) given OR provide response rate OR state that no participants dropped out/declined participation.
Randomization	If participants were not allocated into experimental groups, state so OR describe how participants were allocated to groups, and if allocation was not random, describe how covariates were controlled.

Ecological, evolutionary & environmental sciences study design

All studies must disclose on these points even when the disclosure is negative.

Study description	Briefly describe the study. For quantitative data include treatment factors and interactions, design structure (e.g. factorial, nested, hierarchical), nature and number of experimental units and replicates.
Research sample	Describe the research sample (e.g. a group of tagged Passer domesticus, all Stenocereus thurberi within Organ Pipe Cactus National

Research sample	*Monument), and provide a rationale for the sample choice. When relevant, describe the organism taxa, source, sex, age range and any manipulations. State what population the sample is meant to represent when applicable. For studies involving existing datasets, describe the data and its source.*
Sampling strategy	*Note the sampling procedure. Describe the statistical methods that were used to predetermine sample size OR if no sample-size calculation was performed, describe how sample sizes were chosen and provide a rationale for why these sample sizes are sufficient.*
Data collection	*Describe the data collection procedure, including who recorded the data and how.*
Timing and spatial scale	*Indicate the start and stop dates of data collection, noting the frequency and periodicity of sampling and providing a rationale for these choices. If there is a gap between collection periods, state the dates for each sample cohort. Specify the spatial scale from which the data are taken*
Data exclusions	*If no data were excluded from the analyses, state so OR if data were excluded, describe the exclusions and the rationale behind them, indicating whether exclusion criteria were pre-established.*
Reproducibility	*Describe the measures taken to verify the reproducibility of experimental findings. For each experiment, note whether any attempts to repeat the experiment failed OR state that all attempts to repeat the experiment were successful.*
Randomization	*Describe how samples/organisms/participants were allocated into groups. If allocation was not random, describe how covariates were controlled. If this is not relevant to your study, explain why.*
Blinding	*Describe the extent of blinding used during data acquisition and analysis. If blinding was not possible, describe why OR explain why blinding was not relevant to your study.*

Did the study involve field work? ☐ Yes ☐ No

Field work, collection and transport

Field conditions	*Describe the study conditions for field work, providing relevant parameters (e.g. temperature, rainfall).*
Location	*State the location of the sampling or experiment, providing relevant parameters (e.g. latitude and longitude, elevation, water depth).*
Access & import/export	*Describe the efforts you have made to access habitats and to collect and import/export your samples in a responsible manner and in compliance with local, national and international laws, noting any permits that were obtained (give the name of the issuing authority, the date of issue, and any identifying information).*
Disturbance	*Describe any disturbance caused by the study and how it was minimized.*

Reporting for specific materials, systems and methods

We require information from authors about some types of materials, experimental systems and methods used in many studies. Here, indicate whether each material, system or method listed is relevant to your study. If you are not sure if a list item applies to your research, read the appropriate section before selecting a response.

Materials & experimental systems

n/a	Involved in the study
☐	☐ Antibodies
☐	☐ Eukaryotic cell lines
☐	☐ Palaeontology and archaeology
☐	☐ Animals and other organisms
☐	☐ Human research participants
☐	☐ Clinical data
☐	☐ Dual use research of concern

Methods

n/a	Involved in the study
☐	☐ ChIP-seq
☐	☐ Flow cytometry
☐	☐ MRI-based neuroimaging

Antibodies

Antibodies used	*Describe all antibodies used in the study; as applicable, provide supplier name, catalog number, clone name, and lot number.*
Validation	*Describe the validation of each primary antibody for the species and application, noting any validation statements on the manufacturer's website, relevant citations, antibody profiles in online databases, or data provided in the manuscript.*

Eukaryotic cell lines

Policy information about cell lines

Cell line source(s)	*State the source of each cell line used.*

Authentication	*Describe the authentication procedures for each cell line used OR declare that none of the cell lines used were authenticated.*
Mycoplasma contamination	*Confirm that all cell lines tested negative for mycoplasma contamination OR describe the results of the testing for mycoplasma contamination OR declare that the cell lines were not tested for mycoplasma contamination.*
Commonly misidentified lines (See ICLAC register)	*Name any commonly misidentified cell lines used in the study and provide a rationale for their use.*

Palaeontology and Archaeology

Specimen provenance	*Provide provenance information for specimens and describe permits that were obtained for the work (including the name of the issuing authority, the date of issue, and any identifying information). Permits should encompass collection and, where applicable, export.*
Specimen deposition	*Indicate where the specimens have been deposited to permit free access by other researchers.*
Dating methods	*If new dates are provided, describe how they were obtained (e.g. collection, storage, sample pretreatment and measurement), where they were obtained (i.e. lab name), the calibration program and the protocol for quality assurance OR state that no new dates are provided.*

☐ Tick this box to confirm that the raw and calibrated dates are available in the paper or in Supplementary Information.

Ethics oversight	*Identify the organization(s) that approved or provided guidance on the study protocol, OR state that no ethical approval or guidance was required and explain why not.*

Note that full information on the approval of the study protocol must also be provided in the manuscript.

Animals and other organisms

Policy information about studies involving animals; ARRIVE guidelines recommended for reporting animal research

Laboratory animals	*For laboratory animals, report species, strain, sex and age OR state that the study did not involve laboratory animals.*
Wild animals	*Provide details on animals observed in or captured in the field; report species, sex and age where possible. Describe how animals were caught and transported and what happened to captive animals after the study (if killed, explain why and describe method; if released, say where and when) OR state that the study did not involve wild animals.*
Field-collected samples	*For laboratory work with field-collected samples, describe all relevant parameters such as housing, maintenance, temperature, photoperiod and end-of-experiment protocol OR state that the study did not involve samples collected from the field.*
Ethics oversight	*Identify the organization(s) that approved or provided guidance on the study protocol, OR state that no ethical approval or guidance was required and explain why not.*

Note that full information on the approval of the study protocol must also be provided in the manuscript.

Human research participants

Policy information about studies involving human research participants

Population characteristics	*Describe the covariate-relevant population characteristics of the human research participants (e.g. age, gender, genotypic information, past and current diagnosis and treatment categories). If you filled out the behavioural & social sciences study design questions and have nothing to add here, write "See above."*
Recruitment	*Describe how participants were recruited. Outline any potential self-selection bias or other biases that may be present and how these are likely to impact results.*
Ethics oversight	*Identify the organization(s) that approved the study protocol.*

Note that full information on the approval of the study protocol must also be provided in the manuscript.

Clinical data

Policy information about clinical studies

All manuscripts should comply with the ICMJE guidelines for publication of clinical research and a completed CONSORT checklist must be included with all submissions.

Clinical trial registration	*Provide the trial registration number from ClinicalTrials.gov or an equivalent agency.*
Study protocol	*Note where the full trial protocol can be accessed OR if not available, explain why.*
Data collection	*Describe the settings and locales of data collection, noting the time periods of recruitment and data collection.*
Outcomes	*Describe how you pre-defined primary and secondary outcome measures and how you assessed these measures.*

Dual use research of concern

Hazards

Could the accidental, deliberate or reckless misuse of agents or technologies generated in the work, or the application of information presented in the manuscript, pose a threat to:

No | Yes
☐ | ☐ Public health
☐ | ☐ National security
☐ | ☐ Crops and/or livestock
☐ | ☐ Ecosystems
☐ | ☐ Any other significant area

Experiments of concern

Does the work involve any of these experiments of concern:

No | Yes
☐ | ☐ Demonstrate how to render a vaccine ineffective
☐ | ☐ Confer resistance to therapeutically useful antibiotics or antiviral agents
☐ | ☐ Enhance the virulence of a pathogen or render a nonpathogen virulent
☐ | ☐ Increase transmissibility of a pathogen
☐ | ☐ Alter the host range of a pathogen
☐ | ☐ Enable evasion of diagnostic/detection modalities
☐ | ☐ Enable the weaponization of a biological agent or toxin
☐ | ☐ Any other potentially harmful combination of experiments and agents

ChIP-seq

Data deposition

☐ Confirm that both raw and final processed data have been deposited in a public database such as [GEO](#).

☐ Confirm that you have deposited or provided access to graph files (e.g. BED files) for the called peaks.

Data access links
May remain private before publication.
For "Initial submission" or "Revised version" documents, provide reviewer access links. For your "Final submission" document, provide a link to the deposited data.

Files in database submission
Provide a list of all files available in the database submission.

Genome browser session
(e.g. [UCSC](#))
Provide a link to an anonymized genome browser session for "Initial submission" and "Revised version" documents only, to enable peer review. Write "no longer applicable" for "Final submission" documents.

Methodology

Replicates
Describe the experimental replicates, specifying number, type and replicate agreement.

Sequencing depth
Describe the sequencing depth for each experiment, providing the total number of reads, uniquely mapped reads, length of reads and whether they were paired- or single-end.

Antibodies
Describe the antibodies used for the ChIP-seq experiments; as applicable, provide supplier name, catalog number, clone name, and lot number.

Peak calling parameters
Specify the command line program and parameters used for read mapping and peak calling, including the ChIP, control and index files used.

Data quality
Describe the methods used to ensure data quality in full detail, including how many peaks are at FDR 5% and above 5-fold enrichment.

Software
Describe the software used to collect and analyze the ChIP-seq data. For custom code that has been deposited into a community repository, provide accession details.

Flow Cytometry

Plots

Confirm that:

☐ The axis labels state the marker and fluorochrome used (e.g. CD4-FITC).

☐ The axis scales are clearly visible. Include numbers along axes only for bottom left plot of group (a 'group' is an analysis of identical markers).

☐ All plots are contour plots with outliers or pseudocolor plots.

☐ A numerical value for number of cells or percentage (with statistics) is provided.

Methodology

Sample preparation	*Describe the sample preparation, detailing the biological source of the cells and any tissue processing steps used.*
Instrument	*Identify the instrument used for data collection, specifying make and model number.*
Software	*Describe the software used to collect and analyze the flow cytometry data. For custom code that has been deposited into a community repository, provide accession details.*
Cell population abundance	*Describe the abundance of the relevant cell populations within post-sort fractions, providing details on the purity of the samples and how it was determined.*
Gating strategy	*Describe the gating strategy used for all relevant experiments, specifying the preliminary FSC/SSC gates of the starting cell population, indicating where boundaries between "positive" and "negative" staining cell populations are defined.*

☐ Tick this box to confirm that a figure exemplifying the gating strategy is provided in the Supplementary Information.

Magnetic resonance imaging

Experimental design

Design type	*Indicate task or resting state; event-related or block design.*
Design specifications	*Specify the number of blocks, trials or experimental units per session and/or subject, and specify the length of each trial or block (if trials are blocked) and interval between trials.*
Behavioral performance measures	*State number and/or type of variables recorded (e.g. correct button press, response time) and what statistics were used to establish that the subjects were performing the task as expected (e.g. mean, range, and/or standard deviation across subjects).*

Acquisition

Imaging type(s)	*Specify: functional, structural, diffusion, perfusion.*
Field strength	*Specify in Tesla*
Sequence & imaging parameters	*Specify the pulse sequence type (gradient echo, spin echo, etc.), imaging type (EPI, spiral, etc.), field of view, matrix size, slice thickness, orientation and TE/TR/flip angle.*
Area of acquisition	*State whether a whole brain scan was used OR define the area of acquisition, describing how the region was determined.*

Diffusion MRI ☐ Used ☐ Not used

Preprocessing

Preprocessing software	*Provide detail on software version and revision number and on specific parameters (model/functions, brain extraction, segmentation, smoothing kernel size, etc.).*
Normalization	*If data were normalized/standardized, describe the approach(es): specify linear or non-linear and define image types used for transformation OR indicate that data were not normalized and explain rationale for lack of normalization.*
Normalization template	*Describe the template used for normalization/transformation, specifying subject space or group standardized space (e.g. original Talairach, MNI305, ICBM152) OR indicate that the data were not normalized.*
Noise and artifact removal	*Describe your procedure(s) for artifact and structured noise removal, specifying motion parameters, tissue signals and physiological signals (heart rate, respiration).*

Volume censoring | *Define your software and/or method and criteria for volume censoring, and state the extent of such censoring.*

Statistical modeling & inference

Model type and settings | *Specify type (mass univariate, multivariate, RSA, predictive, etc.) and describe essential details of the model at the first and second levels (e.g. fixed, random or mixed effects; drift or auto-correlation).*

Effect(s) tested | *Define precise effect in terms of the task or stimulus conditions instead of psychological concepts and indicate whether ANOVA or factorial designs were used.*

Specify type of analysis: ☐ Whole brain ☐ ROI-based ☐ Both

Statistic type for inference
(See Eklund et al. 2016) | *Specify voxel-wise or cluster-wise and report all relevant parameters for cluster-wise methods.*

Correction | *Describe the type of correction and how it is obtained for multiple comparisons (e.g. FWE, FDR, permutation or Monte Carlo).*

Models & analysis

n/a	Involved in the study
☐	☐ Functional and/or effective connectivity
☐	☐ Graph analysis
☐	☐ Multivariate modeling or predictive analysis

Functional and/or effective connectivity | *Report the measures of dependence used and the model details (e.g. Pearson correlation, partial correlation, mutual information).*

Graph analysis | *Report the dependent variable and connectivity measure, specifying weighted graph or binarized graph, subject- or group-level, and the global and/or node summaries used (e.g. clustering coefficient, efficiency, etc.).*

Multivariate modeling and predictive analysis | *Specify independent variables, features extraction and dimension reduction, model, training and evaluation metrics.*